Numerical simulation of rime ice accretions on an aerofoil using an Eulerian method

Y. Cao and Q. Zhang
Institute of Aircraft Design
Beijing University of Aeronautics and Astronautics
Beijing, China

J. Sheridan
Department of Mechanical and Aerospace Engineering
Faculty of Engineering
Monash University
Australia

ABSTRACT

Based on two-phase flow theory, an Eulerian method to simulate rime ice accretions on an aerofoil has been developed. The SIMPLE (semi-implicit method for pressure linked equations) algorithm on a collocated grid is employed to solve the governing equations for the airflow. In order to simulate droplets impinging on an aerofoil, a permeable wall is proposed to solve the governing equations for supercooled droplets. The collection efficiency and impingement limits are obtained from the droplets' flowfield. The process of ice accretion is simulated using the assumption that ice accumulates layer-by-layer and the ice shape is predicted with the assumption that ice grows in the direction normal to the aerofoil surface. The rime ice accretions on a NACA0012 aerofoil at 0° and 4° angles-of-attack have been investigated and there is agreement between the simulated results and previously published experimental data. The change of the pressure coefficient along the iced aerofoil is also analysed.

NOMENCLATURE

A	impingement area of control volume
C_D	drag coefficient of droplets
C_P	pressure coefficient
F_D	drag of droplets caused by airflow
F_{GB}	resultant force of the gravity and buoyancy of droplets
g	acceleration of gravity
J	Jacobi factor for co-ordinates transformation
k	turbulent kinetic energy
LWC	liquid water content
m_{WATER}	water flux on an aerofoil surface
MVD	median volumetric diameter
$\mathbf{n}$	normal vector
p	static pressure
Q	generalised variable
Re_W	Reynolds number of droplets
S	source term
u	air velocity
U	droplet contravariant velocity along ξ direction
$\mathbf{U}$	air velocity vector
v	droplet velocity
V	droplet contravariant velocity along η direction
V_{ICE}	ice volume
ΔT	ice accretion time step
α_V	droplet volume fraction
β	local collection efficiency
ε	turbulent dissipation rate
ϕ	generalised variable
μ	molecular viscosity coefficient
ρ	density

Paper No. 3230. Manuscript received 21 August 2007, revised 14 March 2008, accepted 17 March 2008.

$\bar{\rho}$ droplet apparent density
ξ, η co-ordinate components in body-fitted curvilinear co-ordinates
Γ diffusion coefficient
Ω control volume in body-fitted curvilinear co-ordinates

Subscipts

A air value
I ice value
n along normal direction
w wall boundary value
W water value
x, y along x, y directions
∞ free stream value

1.0 INTRODUCTION

In the flight of aeroplanes ice accretions can be found on the wing surface because of the impingement of supercooled droplets. Thus, the designed aerodynamic shape of the wing surface will be changed by the ice accretions such that the aerodynamic performance degrades and the flight safety can be deleteriously affected.

In general, ice accretion is investigated by three means: experiments, engineering methods and numerical simulation. Experiments[1,2] can obtain ice shapes directly but can be very expensive. Engineering methods employ empirical formulae and representative experimental data to investigate the ice accretions, meaning that the process of the ice accretion is difficult to analyse [3,4]. As a result of these impediments, numerical simulation is widely utilised to predict ice accretion.

The numerical simulation methods used to investigate the ice accretion can involve the Lagrangian method[5-7] or Eulerian method[8,9]. The former method has been used for a long time and tracks every droplet in the flowfield by solving its motion equation, based on the velocity distribution of the airflow. The ice accretions can be simulated based on the collection efficiency, i.e. the normalised flux of the droplets on the aerofoil surface, and the impingement limits on the aerofoil surface. The Eulerian method regards the flow of air and droplets as a two-phase flow. The droplet flowfield is obtained by solving the governing equations of the two-phase flow so as to get the collection efficiency and impingement limits on the aerofoil surface. The ice shapes can then be predicted based on these quantities. Thus, the same results can be obtained with the two methods. However, a number of advantages can be found in using the Eulerian method. This method can use the same grid to solve the governing equations for both the airflow and the supercooled droplets. More importantly, the collection efficiency and impingement limits on the aerofoil surface can be obtained from the droplets' flowfield directly, which is a significant advantage in the study of ice accretion on multi-element aerofoils and in three-dimensional ice shape investigations.

There are a number of existing ice accretion codes in the world such as: LEWICE[10], DRA (called TRAJICE 2)[11], FENSAP-ICE[12], ONERA[13] and CIRAML[14]. The code FENSAP-ICE employs the Eulerian method while the other four codes employ the Lagrangian method.

Based on two-phase flow theory, an Eulerian method to numerically simulate rime ice accretions on an aerofoil is developed in this paper. The SIMPLE algorithm[15] on a collocated grid is employed to solve the air flowfield. The governing equations for droplets are solved by proposing a permeable wall to simulate droplet impingement on the aerofoil surface. Then the collection efficiency and impingement limits can be obtained directly from the droplet flowfield. The ice accretion is simulated with the assumption that ice accumulates layer-by-layer and the ice shape is predicted with the assumption that ice grows in the direction normal to the aerofoil surface. This model has then been used to study the change of the pressure coefficient along the aerofoil resulting from the presence of the ice accretion.

2.0 GOVERNING EQUATIONS OF TWO-PHASE FLOWS

The following assumptions are needed before the governing equations of two-phase flows are established:

1. The volume fraction of droplets is so small that the effect of the droplet movement on airflow can be neglected.
2. The external forces imposed on the droplets only involve the drag, arising from the airflow, gravity and buoyancy. The turbulent fluctuations of the airflow have no effect on the droplet movement.
3. There is no heat transfer or evaporation during the droplet movement. Thus, the physical parameters of the droplets are assumed not to change.
4. The droplets are simplified to be spheres with a median volumetric diameter.

2.1 Governing equations for airflow

According to Assumption 1, there is no coupling relationship between the governing equations for the airflow and droplets, meaning that the governing equations for the airflow can be solved independently. The 2D steady and incompressible Reynolds-averaged Navier-Stokes equations with a $k - \varepsilon$ turbulent model can be written as:

$$\mathrm{div}(\rho_A \mathbf{U}\phi) = \mathrm{div}(\Gamma_\phi \mathrm{grad}\phi) + S_\phi \quad \ldots (1)$$

where, ϕ = 1, u_x, u_y, k, ε in the continuity equation, momentum equations, turbulent kinetic energy equation and turbulent dissipation rate equation respectively. u_x, u_y, k and ε denote the air velocities along x, y direction, turbulent kinetic energy and turbulent dissipation rate respectively. The symbols ρ_A, $\mathbf{U}$, Γ_ϕ and S_ϕ denote the air density, air velocity vector, diffusion coefficient and source terms respectively.

2.2 Solution of the governing equations for the airflow

In order to solve the governing equations for the airflow, the boundary conditions can be set as follows:

1. Velocity inlet boundary: if this boundary is far from the aerofoil the infinite conditions can be employed and the static pressure p can be obtained by a second-order extrapolation.
2. Wall boundary: the no-slip condition is employed so that u_x and u_y are equal to zero in the wall while k and ε can be set using the wall function[16]. The static pressure can be obtained with the condition $\partial p/\partial \mathbf{n} = 0$.
3. Outflow boundary: all variables satisfy the condition $\partial Q/\partial \mathbf{n} = 0$, where Q denotes variables u_x, u_y, p, k, ε.

This paper makes the air velocities u_x, u_y and static pressure p as the original variables, and uses the SIMPLE algorithm on a collocated grid to solve the governing equations for the airflow. The momentum interpolation is utilised to establish the pressure correction equation, which overcomes the problem of the velocity-pressure decoupling. The governing equations are discretised using the finite-volume method. The convective term is discretised using the QUICK (quadratic upwind interpolation of convective kinematics) scheme[17], and the deferred correction method is used to ensure the diagonal dominance in the discretised equations. The ADI (alternating direction implicit) method[18] is used to solve the discretised equations.

2.3 Governing equations for droplets

Based on the multi-fluid model of droplets[19], the droplets distributed in the flowfield can be regarded as a kind of pseudo fluid that penetrates the 'real' fluid in Eulerian co-ordinates. According to Assumptions 2, 3 and 4, the fluctuation term, phase-change term and Magnus force in the governing equations for droplets can be neglected. Furthermore, the energy equation needs not to be solved.

Therefore, the continuity and momentum equations for the droplets can be simplified as:

$$\frac{\partial \bar{\rho}}{\partial t}+\frac{\partial(\bar{\rho} v_j)}{\partial x_j}=0 \qquad \ldots (2)$$

$$\frac{\partial(\bar{\rho} v_i)}{\partial t}+\frac{\partial(\bar{\rho} v_j v_i)}{\partial x_j}=F_{Di}+F_{GBi} \qquad \ldots (3)$$

$(i, j = 1, 2)$

In above equations, $\bar{\rho}$ denotes droplet apparent density (i.e. the mass of droplets per unit volume) and $\bar{\rho} = \alpha_V \cdot \rho_W$, where α_V, ρ_W denote the droplet volume fraction and density of water respectively. The symbols v_i, F_{Di}, F_{GBi} denote the droplet velocities, drag caused by airflow, and the resultant force of the gravity and buoyancy of droplets respectively.

The formula for calculating F_{Di} can be written as:

$$F_{Di}=\frac{0\cdot 75\bar{\rho}\cdot C_D \mathrm{Re}_W \cdot \mu}{\rho_W \cdot MVD^2}\left(u_i - v_i\right) \qquad \ldots (4)$$

where, u_i is the air velocity. The symbols μ, MVD, C_D, Re_W denote the molecular viscosity coefficient, median volumetric diameter, drag coefficient and Reynolds number of the droplets respectively. The expression of Re_W can be written as:

$$\mathrm{Re}_W=\frac{\rho_A \cdot MVD}{\mu}\left|u-v\right| \qquad \ldots (5)$$

Furthermore, the combined variable $C_D\mathrm{Re}_W$ can be calculated with the following formula[20]:

$$C_D\mathrm{Re}_W = 24(1+0\cdot 197\mathrm{Re}_W^{0.63}+2\cdot 6\times 10^{-4}\mathrm{Re}_W^{1.38}) \qquad \ldots (6)$$

The formula calculating F_{GBi} can be written as:

$$F_{GBi}=\bar{\rho}\cdot g_i\left(1-\frac{\rho_A}{\rho_W}\right) \qquad \ldots (7)$$

where g_i is the acceleration due to gravity.

2.4 Simulation of droplet impingement on an aerofoil surface through a permeable wall

The velocity inlet boundary condition of the droplet flowfield can be set as follows: the droplet velocity is the same as the air velocity of the free stream, and the droplet apparent density is equal to the liquid water content of the free stream.

At the outflow boundary, all variables satisfy the condition $\partial Q/\partial \mathbf{n} = 0$, where Q denotes all variables in the governing equations for droplets.

In the Eulerian method, the collection efficiency is determined by the droplet apparent density and velocity near the wall. Therefore, the setting of the wall condition is an important factor in the solution of the droplet flowfield.

Some previous literatures[8,12] set the initial values of the droplet apparent density and velocity near the wall to be zero, and no special techniques were employed to deal with the wall boundary. This can cause oscillations in the solution of the droplet flowfield and some extra stabilisation terms must be added.

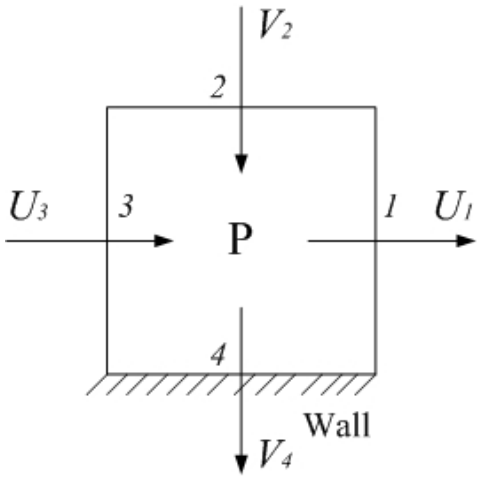

Figure 1. Contravariant velocity distribution of the control volume.

The approach taken in this paper is to use a permeable wall to simulate droplet impingement on the aerofoil surface. First, Cartesian coordinates are transformed into body-fitted curvilinear co-ordinates and, in order to illustrate the problem conveniently, a control volume near the stagnation point of the aerofoil is selected as the investigated object, as shown in Fig. 1.

From Fig. 1, the control volume has four interfaces with corresponding droplet velocities. These velocities are contravariant velocities[21] in body-fitted curvilinear co-ordinates and they are perpendicular to corresponding interfaces. The contravariant velocities U_1 and U_3 in interface 1 and interface 3 are parallel to the wall boundary. Therefore, they do not contribute to the impingement. On the other hand, the contravariant velocity V_2 in interface 2 points to the interior of the control volume, which means that droplets will flow into the control volume through interface 2.

If the droplet velocity on the wall boundary (which is a superposition to interface 4 of the control volume) is set to be zero, the droplet contravariant velocity V_4 is equal to zero. Therefore, in the discretisation process using the finite-volume method, this setting is equivalent to a fact that droplets have no impingement with the wall because the net flux of droplets into interface 4 (namely the wall boundary) is null. As a result, most of the droplets which flow into the control volume through interface 2 settle in the control volume and can not reach the wall. In this way the method can not simulate the physical phenomenon of the impingement between the droplets and wall effectively.

In fact, because of the means of the impingement between the droplets and wall, the supercooled droplets adhere to the wall after they have inelastic impingements with the wall and then turn into ice. However, before the droplets reach the wall, they have fairly high normal velocity relative to the wall and this velocity turns into zero instantaneously when the droplets impinge with the wall inelastically.

Similarly, the droplet apparent density on the wall boundary can not be set to be zero, otherwise it is equivalent to the fact that no droplets will impinge on the wall.

Based on the above analysis and by also taking into account the principle that droplets can not flow into the interior flowfield from the wall it is possible to set the wall condition as follows:

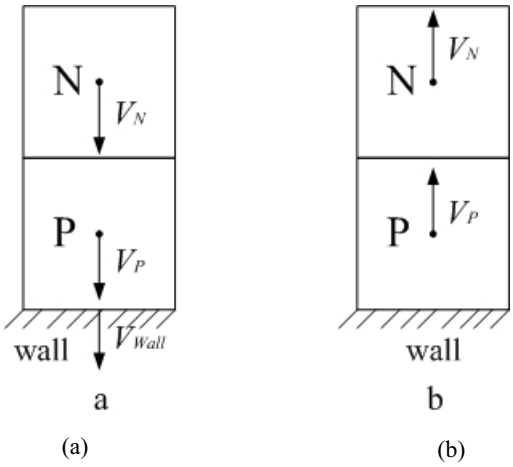

(a) (b)

Figure 2. Setting of the wall boundary conditions.

If the contravariant velocity V_P, located in the centre of a control volume near the wall, points to the wall, the droplets within this control volume may impinge onto the wall (as shown in Fig. 2(a)). Then the contravariant velocity on the wall boundary is calculated through an interpolation from the interior flowfield, as is the apparent density on the wall boundary. These contravariant velocity and apparent density are applied as the wall condition for this control volume in the next iteration.

If, however, the contravariant velocity V_P in the center of the control volume near the wall points to the interior flowfield, the droplets have no possibility of impinging on the wall (as shown in Fig. 2(b)). In this case the droplet velocity and apparent density on the wall boundary are set to be zero, which is applied as the wall condition for this control volume in the next iteration.

The droplet impingement on an aerofoil surface can be simulated effectively by applying this wall condition and the accuracy and convergence of the numerical computation can also be improved.

2.5 Solution of the governing equations for droplets

In 2D applications there are three unknown variables — the droplet velocities and apparent density. The equations can be solved in closed form because the number of unknowns is equal to the number of equations. First, Cartesian co-ordinates are transformed into a set of body-fitted curvilinear co-ordinates and the governing equations are discretised using the finite-volume method. The convective term is discretised using the QUICK scheme, with the deferred correction method employed. The temporal term is discretised using the first-order implicit scheme.

The droplet apparent density and velocities at time t^n are solutions of

$$J\frac{\bar{\rho}^n-\bar{\rho}^{n-1}}{\Delta t}+\iint_\Omega\left[\frac{\partial}{\partial\xi}(\bar{\rho}U)^n+\frac{\partial}{\partial\eta}(\bar{\rho}V)^n\right]d\xi d\eta=0 \qquad \ldots(8)$$

$$J\frac{(\bar{\rho}v_i)^n-(\bar{\rho}v_i)^{n-1}}{\Delta t}+\iint_\Omega\left[\frac{\partial}{\partial\xi}(\bar{\rho}Uv_i)^n+\frac{\partial}{\partial\eta}(\bar{\rho}Vv_i)^n\right]d\xi d\eta=\iint_\Omega\left[J(F_{Di}+F_{GBi})^n\right]d\xi d\eta \qquad \ldots(9)$$

$$(i=1,2)$$

where Ω, J and U, V denote the control volume in body-fitted curvilinear co-ordinates, Jacobi factor and droplet contravariant velocity components, respectively.

It is worth noting that the possible oscillations in the solution of the governing equations for droplets mentioned in Ref. 8 and Ref. 12 are not found using the computational method presented in this paper. Therefore, the extra stabilisation terms are not needed.

3.0 PREDICTION OF ICE ACCRETIONS

3.1 Ice volume calculation on an aerofoil

Based on the velocity distribution of airflow over an aerofoil, the governing equations for the droplets are solved and the normal velocity v_{nw} and apparent density $\bar{\rho}_w$ of droplets on the wall boundary can be obtained after the numerical computation converges. Therefore, the local collection efficiency β, which is non-dimensional, can be obtained conveniently with the Eulerian method:

$$\beta=\frac{\bar{\rho}_w\cdot v_{nw}}{LWC\cdot v_\infty} \qquad \ldots(10)$$

where, LWC, v_∞ denote the liquid water content and the droplets' velocity in the free stream.

The water flux m_{WATER} on the aerofoil surface can be calculated with the following expression:

$$m_{WATER}=LWC\cdot v_\infty\cdot\beta\cdot A \qquad \ldots(11)$$

where, A denotes the impingement area of a control volume near the wall.

The rime ice simulated in this paper forms in an environment with a low temperature and where supercooled droplets freeze instantaneously when they impinge onto the aerofoil surface. Therefore, the ice volume V_{ICE} can be calculated as:

$$V_{ICE}=\frac{m_{WATER}\cdot\Delta T}{\rho_I} \qquad \ldots(12)$$

where, ΔT and ρ_I denote the ice accretion time step and the density of the ice.

3.2 Ice shape prediction

According to the ice volume, the ice shape after a time step can be predicted with the assumption that ice grows in the direction normal to the aerofoil surface. When the aerofoil shape is changed by the ice accretion, the air flowfield is changed as a result. Therefore, the air flowfield needs to be re-solved, as do the governing equations for the droplets. The new ice shape can then be predicted based on the solution of the governing equations for the droplets. The final shape of the ice accretion can be obtained by repeating this iterative process over a number of time steps until the end of ice accretion time.

4.0 RESULTS AND ANALYSIS

The technique outline above has been applied to rime ice accretions on a NACA0012 aerofoil at 0° and 4° angles-of-attack.

Figure 3 shows the computational mesh of the clear aerofoil.

4.1 Ice shape prediction at 0° angle-of-attack

The computational conditions are: the velocity of the free stream u_∞ = 129ms^{-1}, the static pressure p_∞ = 101,300Pa, the liquid water content LWC = 0·5g/m^3, the median volumetric diameter MVD =

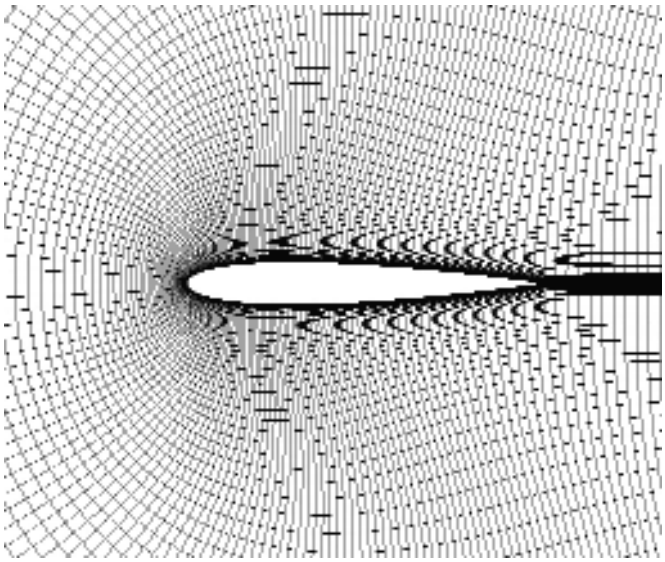

Figure 3. Computational mesh of the clear aerofoil.

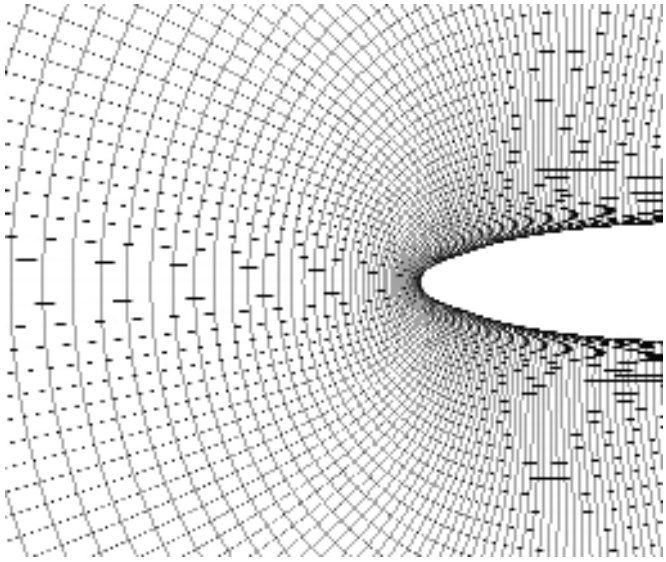

Figure 4. Computational mesh of the iced aerofoil at 0° angle-of-attack.

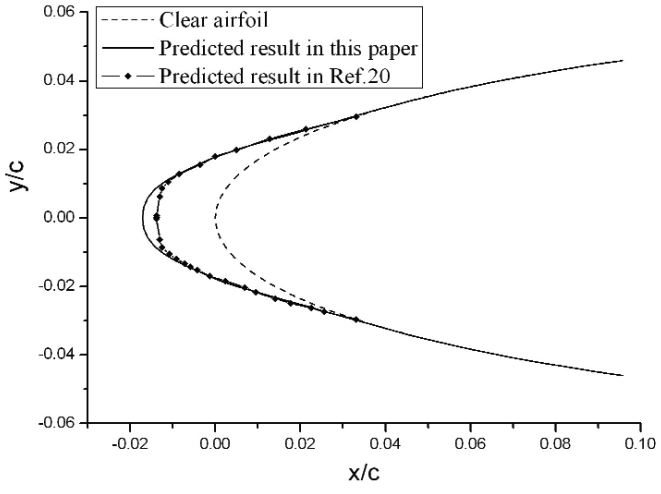

Figure 5. Comparison of the predicted results at 0° angle-of-attack.

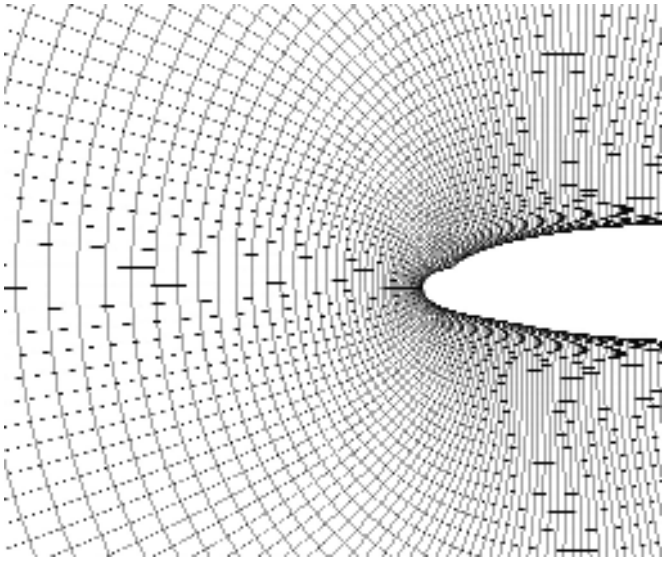

Figure 6. Computational mesh of the iced aerofoil at 4° angle-of-attack.

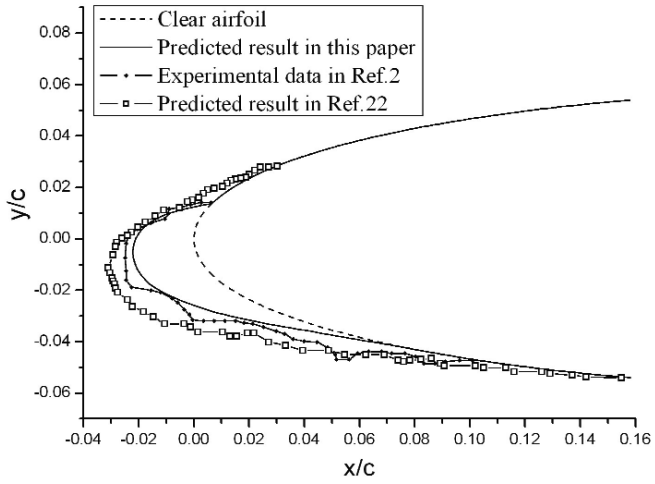

Figure 7. Comparison of the ice shapes at 4° angle-of-attack.

20μm and the ice accretion time is selected to be 300 seconds. Figure 4 shows the computational mesh of the iced aerofoil at 0° angle-of-attack. Figure 5 shows the comparison between the predicted results in this paper and in Ref. 20 under similar icing conditions.

As shown in Fig. 5, there appears to be good agreement in the predictions of the icing area between this paper and Ref. 20, while the maximum ice thickness in this paper is larger than in Ref. 20.

4.2 Ice shape prediction at 4° angle-of-attack

The computational conditions are: the velocity of the free stream u_∞ = 67 ms^{-1}, the static pressure p_∞= 101,300Pa, the liquid water content LWC = 1·0g/m^3, the median volumetric diameter MVD = 20μm and the ice accretion time is selected to be 360 seconds.

Figure 6 shows the computational mesh of the iced aerofoil at 4° angle-of-attack. Figure 7 shows the comparison between the predicted results from this work, those presented in Ref. 22 and the experimental data presented in Ref. 2 under similar icing conditions.

As shown in Fig. 7, both the predicted results from this work and from Ref. 22 show some slight variation with the experimental data.

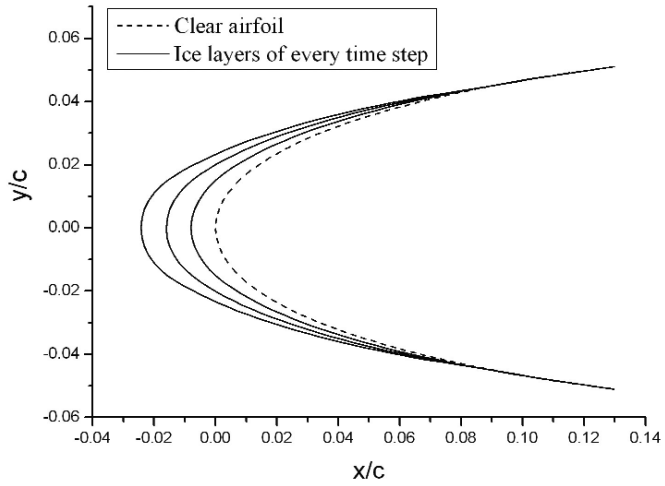

Figure 8. Ice layers of 60 seconds, 120 seconds and 180 seconds when *MVD* = 50μm.

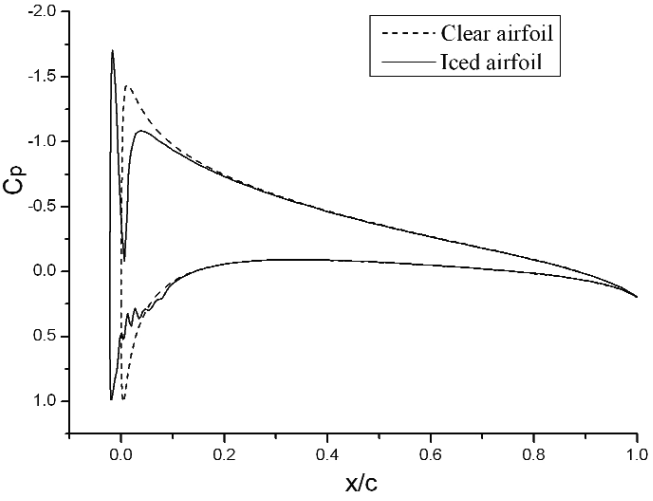

Figure 9. Comparison of pressure coefficient distributions between the

However, the results from this paper are somewhat closer to the experimental data than those from Ref. 22. While the icing area on the lower surface of the aerofoil is smaller than that found in the experimental data, the icing area on the upper surface and the ice thickness predicted in this work agree well with the experimental data. Both the ice thickness and icing area predicted in Ref. 22 are somewhat larger than the experimental data.

4.3 Analysis of the predicted results

From Fig. 5 it can be seen that at 0° angle-of-attack the predicted ice shape is almost symmetrical about the aerofoil chord, as would be expected due to the symmetry of the flow. This is also the explanation for why the maximum thickness of ice is found at the leading edge of the aerofoil. When the angle-of-attack is equal to 4 degrees, Fig. 7 shows that the stagnation point of the airflow and the impingement area of the droplets move to the lower surface of the aerofoil. Accordingly, the ice is mostly found on the lower surface while there is little ice on the upper surface. Furthermore, the maximum ice thickness is also found on the lower surface.

4.4 Effect of the median volumetric diameter of droplets on ice accretions

To investigate the effect of the median volumetric diameter of droplets on the ice accretion, this paper shows predictions of the ice shape when the *MVD* is equal to 50μm at 0° angle-of-attack. The other icing conditions are: u_∞ = 129ms^{-1}, p_∞ = 101,300Pa, *LWC* = 1·0g/m^3 and the ice accretion time is selected to be 180 seconds.

Figure 8 shows the ice layers in three time steps of one minute. From the figure, it can be seen that the icing area increases with increasing median volumetric diameter of the droplets. The icing limits on the upper and lower surfaces of the aerofoil now extend to about 8·6% of the chord. Furthermore, the ice grows quickly; the maximum ice thickness has grown to 2·6% of the chord at 180 seconds. The reason for this is explained by the fact that the droplets with a larger diameter have larger inertia than the ones with a smaller diameter. Therefore, the movements of the larger droplets are less affected by the airflow and so their trajectories do not depart from the aerofoil surface easily, which causes the larger icing area and thicker ice.

4.5 Effect of ice accretions on pressure distribution along the aerofoil

Based on the predicted result at 4° angle-of-attack, the change of the pressure coefficient C_P along the iced aerofoil has been analysed. As shown in Fig. 7, the ice accretion alters and corrupts the designed aerodynamic shape of the aerofoil and the ice is mostly found on its lower surface because of the effect of the angle-of-attack. However, the ice accretion has a greater effect in corrupting the designed aerodynamic shape of the leading edge on the upper surface and does so to the extent that a separation bubble can emerge.

Figure 9 shows the comparison of the pressure coefficient distributions between the clear aerofoil and iced aerofoil at 4° angle-of-attack. From the figure, we can see that oscillations can be found in the pressure coefficient curves on both the upper surface and lower surface of the iced aerofoil. Near the leading edge on the upper surface, the curve oscillates acutely because of the great corruption of the designed aerodynamic shape caused by the ice accretion. On the lower surface, the oscillation region is wider because of the wider icing area. However, the pressure coefficient curve of the lower surface oscillates more weakly than the one of the upper surface because the ice accretion on the lower surface is smoother.

From Fig. 9, it can be seen that the pressure distribution is changed by the variation of the aerofoil shape caused by the ice accretion. This will result in a degradation of the aerofoil's aerodynamic performance.

5.0 CONCLUSIONS

This paper simulates rime ice accretions on an aerofoil using an Eulerian method based on two-phase flow theory. A permeable wall is used to simulate the droplets' impingement on the aerofoil surface. Based on the approach outlined, the governing equations for droplets are solved to obtain the collection efficiency and impingement limits on the aerofoil surface. This is then used to predict the ice accretion. Some conclusions can be drawn from an investigation of the ice accretion on a NACA0012 aerofoil:

1. In the two-dimensional icing problem, it is feasible and effective to numerically simulate rime ice accretions on an aerofoil using an Eulerian method. Furthermore, the collection efficiency and impingement limits on the aerofoil surface can be obtained more conveniently than by the traditional Lagrange method.
2. The ice shapes vary depending on the angle-of-attack. The ice accretion time, liquid water content and median volumetric diameter of the droplets all have effects on the ice accretion.

3. Ice accretions can degrade the aerofoil's aerodynamic performance. Furthermore, the shape of real ice will be more irregular than the simulated one and the surface of the real ice will be rougher, as can be seen in Fig. 7. Therefore, the degradation of the aerodynamic performance in reality will be greater than that shown here. Furthermore, the degradation caused by rime ice, as studied in this paper, is relatively weak compared with that caused by the glaze ice.

REFERENCES

1. ADDY, H.E., POTAPCZUK, J.M.G. and SHELDON, D.W. Modern airfoil ice accretions, 1997, AIAA paper 0174.
2. SHIN, J. and BOND, T.H. Results of an icing test on a NACA 0012 airfoil in the NASA Lewis Icing Research Tunnel, 1992, AIAA paper 0647.
3. BOWDEN, D.T., GENSEMER, A.G. and SHEEN, C.A. Engineering summary of airframe icing technical data, 1963, FAA Technical Report ADS-4.
4. WILDER, R.W. A theoretical and experimental means to predict ice accretion shapes for evaluation aircraft handling and performance characteristics, 1977, Paper 5, AGARD Advisory Report 127.
5. PARASCHIVOIU, I., TRAN, P. and BRAHIMI, M.T. Prediction of the ice accretion with viscous effects on aircraft wings, 1993, AIAA paper 0027.
6. CARUSO, S.C. Three-dimensional unstructured mesh procedure for iced wing flowfield and droplet trajectory calculations, 1994, AIAA paper 0486.
7. FREGEAU, M., SAEED, F. and PARASCHIVOIU, I. Surface heat transfer study for ice accretion and anti-icing prediction in three dimension, 2004, AIAA paper 0063.
8. BOURGAULT, Y., HABASHI, W.G., DOMPIERRE, J. and BOUTANIOS, Z. An Eulerian approach to supercooled droplets impingement calculations, 1997, AIAA paper 0176.
9. KAZUHIRO, T. Numerical simulation of ice accretion on a body with droplet flow model, 1999, AIAA paper 3333.
10. RUFF, G.A. and BERKOWITZ, B.M. Users manual for the NASA Lewis ice accretion prediction code (LEWICE), 1990, NASA CR 185129.
11. GENT, R.W. TRAJICE2 — A combined water droplet trajectory and ice accretion prediction program for aerofoils, 1990, RAE TR 90054.
12. BEAUGENDRE, H., MORENCY, F. and HABASHI, W.G. FENSAP-ICE's three-dimensional in-flight ice accretion module: ICE3D, *J Aircr*, 2003, **40**, (2), pp 239-247.
13. HEDDE, T. and GUFFOND, D. ONERA three-dimensional icing model, *AIAA J*, 1995, **33**, (6), pp 1038-1045.
14. MINGIONE, G., BRANDI, V. and ESPOSITO, B. Ice accretion prediction on multi-element airfoils, 1997, AIAA paper 0177.
15. PATANKAR, S.V., and SPALDING, D.B. A calculation procedure for heat, mass and momentum transfer in three-dimensional parabolic flow, *Int J Heat Mass Transfer*, 1972, **15**, pp 1787-1806.
16. LAUNDER, B.E. and SPALDING, D.B. The numerical computation of turbulent flows, *Computer Methods in App Mech and Engineering*, 1974, **3**, pp 269-289.
17. LEONARD, B.P. A stable and accurate convective modeling procedure based on quadratic upstream interpolation, *Computer Methods in App Mech and Engineering*, 1979, **19**, pp 59-98.
18. AMES, W.F. *Numerical Methods for Partial Differential Equations*, 1977, Academic Press, New York, USA.
19. ZHOU, L.X. *Theory and Numerical Modeling of Turbulent Gas-Particle Flows and Combustion*, 1993, Science Press and CRC Press, New York.
20. SNELLEN, M., BOELENS, O.J. and HOEIJMAKERS, H.W.M. A computational method for numerically simulating ice accretion, 1997, AIAA Paper 2206.
21. SHYY, W. *Computational Modeling for Fluid Flow and Interfacial Transport*, 1994, Elsevier, Amsterdam.
22. FORTIN, G., ILINCA, A., LAFORTE, J.-L. and BRANDI, V. Prediction of 2D airfoil ice accretion by bisection method and by rivulets and beads modeling, 2003, AIAA paper 1076.